Short Article

Cell Metabolism

Lack of Glycogenin Causes Glycogen Accumulation and Muscle Function Impairment

Graphical Abstract

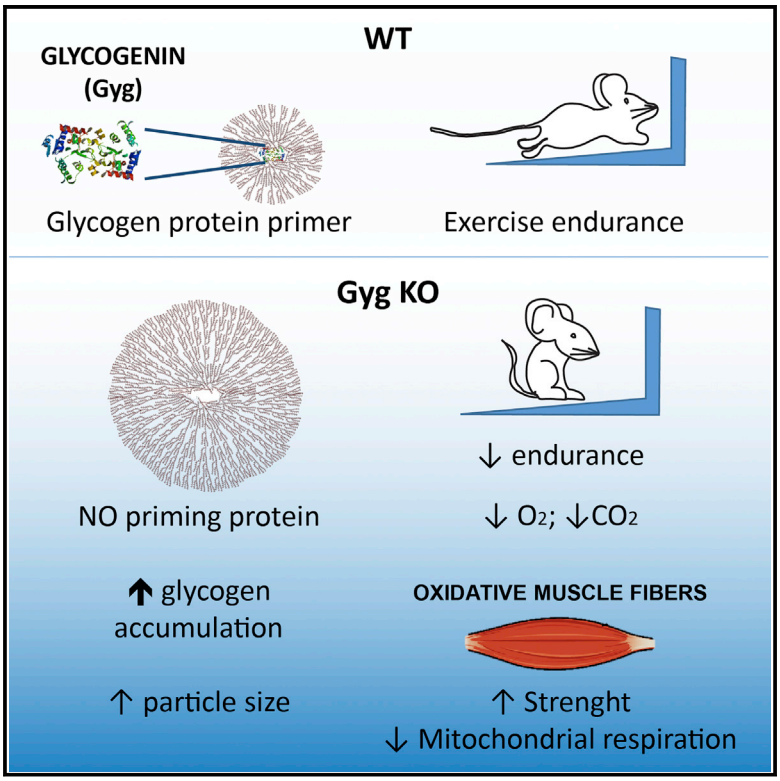

Authors

Giorgia Testoni, Jordi Duran, Mar García-Rocha, ..., Marta Vilaseca, Pura Muñoz-Cánoves, Joan J. Guinovart

Correspondence

guinovart@irbbarcelona.org

In Brief

Although glycogenin is thought to be essential for glycogen synthesis, Testoni et al. show that glycogenin-deficient animals still make glycogen. Surprisingly, glycogen accumulates in striated muscle affecting functionality, including decreased exercise endurance. These findings impact our understanding of glycogen storage disease XV where patients lack glycogenin-1 and accumulate muscle glycogen.

Highlights

- Glycogen synthesis does not require a protein primer
- Glycogenin depletion causes high glycogen accumulation in striated muscles
- Glycogenin depletion alters skeletal muscle functionality
- Over-accumulation of skeletal muscle glycogen affects oxidative metabolism

Testoni et al., 2017, Cell Metabolism *26*, 256–266
July 5, 2017
http://dx.doi.org/10.1016/j.cmet.2017.06.008

CellPress

CellPress

Cell Metabolism
Short Article

Lack of Glycogenin Causes Glycogen Accumulation and Muscle Function Impairment

Giorgia Testoni,[1] Jordi Duran,[1,2] Mar García-Rocha,[1] Francisco Vilaplana,[3] Antonio L. Serrano,[4] David Sebastián,[1,2,5] Iliana López-Soldado,[1,2] Mitchell A. Sullivan,[6] Felipe Slebe,[1] Marta Vilaseca,[1] Pura Muñoz-Cánoves,[4,7,8] and Joan J. Guinovart[1,2,5,9,*]

[1]Institute for Research in Biomedicine (IRB Barcelona), The Barcelona Institute of Science and Technology, Barcelona 08028, Spain
[2]Centro de Investigación Biomédica en Red de Diabetes y Enfermedades Metabólicas Asociadas (CIBERDEM), Madrid 28029, Spain
[3]Division of Glycoscience, School of Biotechnology, KTH Royal Institute of Technology, AlbaNova University Centre, Stockholm 10691, Sweden
[4]Cell Biology Group, Department of Experimental and Health Sciences, Pompeu Fabra University (UPF), CIBER on Neurodegenerative diseases (CIBERNED), Barcelona 08003, Spain
[5]Department of Biochemistry and Molecular Biomedicine, University of Barcelona, Barcelona 08028, Spain
[6]Program in Genetics and Genome Biology, The Hospital for Sick Children, Toronto, ON M5G 1X8, Canada
[7]Institució Catalana de Recerca i Estudis Avançats (ICREA), Barcelona 08010, Spain
[8]Spanish National Center on Cardiovascular Research (CNIC), Madrid 28029, Spain
[9]Lead Contact
*Correspondence: guinovart@irbbarcelona.org
http://dx.doi.org/10.1016/j.cmet.2017.06.008

SUMMARY

Glycogenin is considered essential for glycogen synthesis, as it acts as a primer for the initiation of the polysaccharide chain. Against expectations, glycogenin-deficient mice (Gyg KO) accumulate high amounts of glycogen in striated muscle. Furthermore, this glycogen contains no covalently bound protein, thereby demonstrating that a protein primer is not strictly necessary for the synthesis of the polysaccharide *in vivo*. Strikingly, in spite of the higher glycogen content, Gyg KO mice showed lower resting energy expenditure and less resistance than control animals when subjected to endurance exercise. These observations can be attributed to a switch of oxidative myofibers toward glycolytic metabolism. Mice overexpressing glycogen synthase in the muscle showed similar alterations, thus indicating that this switch is caused by the excess of glycogen. These results may explain the muscular defects of GSD XV patients, who lack glycogenin-1 and show high glycogen accumulation in muscle.

INTRODUCTION

Glycogen is a branched polymer of glucose residues that is stored and later released to meet energy demands. Skeletal muscle comprises a spectrum of fast-twitch glycolytic fibers, which use glycogen as the main source of energy for anaerobic metabolism to fuel short and intense activity (the extensor digitorum longus [EDL] is a muscle rich in this fiber type), and slow-twitch oxidative fibers, which are used for prolonged low-intensity activity (abundant in the soleus) driven primarily by fuels such as blood glucose and fatty acids (Schiaffino and Reggiani, 1996). It is generally accepted that glycogen synthesis is mediated by the action of two enzymes: glycogenin, the primer of the reaction, and glycogen synthase (GS), the elongator of the glucose chain. Glycogenin is a glycosyltransferase that catalyzes the addition of glucose residues to itself. The first glucose is transferred from UDP-glucose to its Tyr195 residue. The following glucose residues are then bound sequentially to form a chain of 10–20 residues (Alonso et al., 1995; Cao et al., 1993; Krisman and Barengo, 1975; Smythe and Cohen, 1991; Whelan, 1986). Further chain elongation is performed by GS, and branches are introduced by the glycogen branching enzyme (GBE). GS interacts directly with the glycosyl-primer chain through the active site and also interacts with the 34 conserved amino acids of glycogenin's C-terminal domain (Zeqiraj et al., 2014). The interaction between GS and glycogenin is considered essential for glycogen synthesis.

In humans and most mammals, glycogenin is present in two isoforms: GYG1, which is widely expressed, and GYG2, which is predominantly expressed in the liver and to a minor degree in cardiac muscle and the pancreas. Recently, a new form of glycogenosis (GSD XV) resulting from GYG1 loss of function has been described. Patients with this condition present with glycogen accumulation and muscle weakness (Malfatti et al., 2014).

Differently from humans, rodents carry a single Gyg gene, which is expressed in all tissues (Mu et al., 1997; Zhai et al., 2001). This characteristic makes *Mus musculus* an ideal model in which to study the impact of glycogenin depletion on glycogen metabolism. To challenge the role of glycogenin, we generated a Gyg knockout mouse model (Gyg KO). Unexpectedly, rather than preventing the synthesis of glycogen, the absence of glycogenin caused glycogen over-accumulation in striated muscles. Remarkably, this glycogen was synthesized without the participation of a substitute protein primer. Furthermore, in spite of the higher muscle glycogen levels, these animals showed impaired endurance muscle performance, a phenotype similar to that of GDS XV patients.

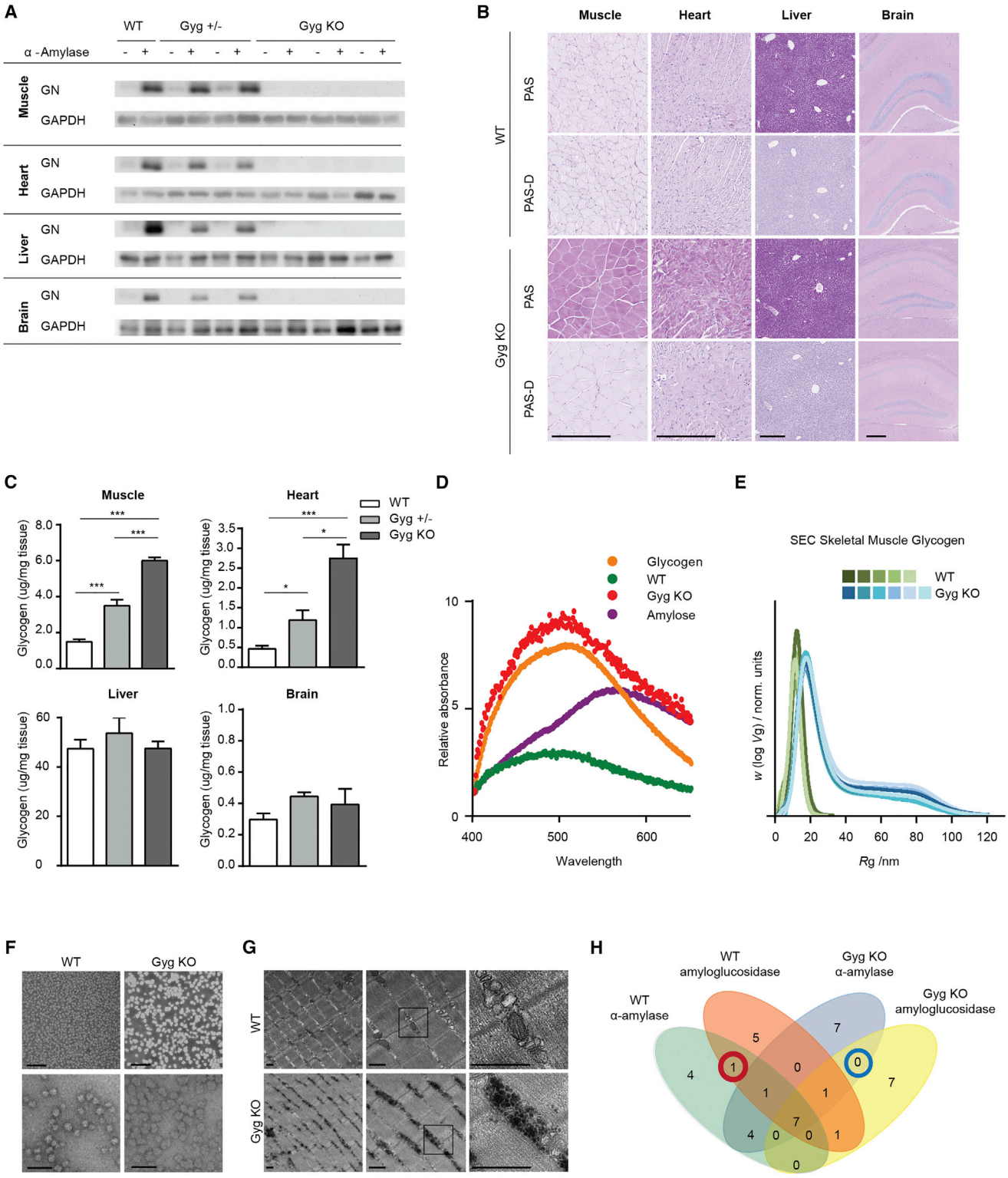

Figure 1. Characterization of Gyg KO Mouse Model and Gyg KO Muscle Glycogen

(A) Immunoblot for glycogenin in the skeletal muscle, heart, liver, and brain of WT, Gyg +/−, and Gyg KO mice. Glycogenin protein is detectable only after treatment with α-amylase, used to degrade covalently bound glycogen and allow entrance in the polyacrylamide gel.

(B) Histological localization of glycogen by PAS staining in the absence or presence of diastase (PAS-D) on paraffin-embedded slides of skeletal muscle, heart, liver, and brain from 15- to 20-week-old males. Scale bar: 250 μm.

(legend continued on next page)

RESULTS

Glycogenin-Deficient Animals Have the Capacity to Synthesize Glycogen

We generated homozygous Gyg KO mice by mating heterozygous mice (Gyg +/−) for the constitutive disruption on the Gyg gene. The genotype was confirmed by western blot and mRNA expression analysis of glycogenin (Figure 1A and Figure S1A). The number of pups per litter was lower than expected, and the proportion of Gyg KO mice was only 4% (lower than the 25% predicted by Mendelian genetics) (Figure S1B). However, the genetic ratio of embryos at E18.5 was in line with Mendelian proportions. Indeed, most of the Gyg KO pups died shortly after birth due to cardiorespiratory failure.

Unexpectedly, Periodic acid-Schiff staining (PAS) and biochemical measurements revealed that Gyg KO mice were able to synthesize glycogen (Figures 1B and 1C). In fact, both the liver and brain contained normal levels of this polysaccharide, while skeletal and cardiac muscle contained four and seven times more glycogen, respectively. Gyg heterozygous mice (carrying one allele of the Gyg gene) showed a moderate increase. Interestingly, the accumulation of glycogen did not increase progressively with age in any tissue (Figure S1C).

To analyze the impact of glycogenin depletion on the two key enzymes of glycogen metabolism, GS and glycogen phosphorylase (GP), we measured their levels and activity in the KO model. In skeletal muscle, the mRNA levels of GS and GP were equal to those found in the controls (Figure S1D), while an increase in protein level and activity was detected (Figure S1E). This indicates that neither glycogen synthesis nor degradation was impaired.

In several glycogen storage diseases (GSDs), such as Lafora disease (LD; EPM2, OMIM254780) and Adult Polyglucosan Bodies disease (APBD, OMIM263570), glycogen is poorly branched and accumulates in the form of amylase-resistant aggregates. However, in the PAS staining of Gyg KO mouse muscle and heart tissue, we observed a uniform distribution of the polysaccharide (Figure 1B). Furthermore, amylase treatment resulted in the complete degradation of glycogen (PAS-D). We also measured the degree of branching by analyzing the spectra of the glycogen-iodine complex. Gyg KO glycogen gave the same absorbance peak as commercial glycogen and purified glycogen from WT animals (Figure 1D). This indicates that glycogen synthesized by Gyg KO animals shows a normal degree of branching. We also characterized the size of the particles using size-exclusion chromatography (SEC). This analysis revealed that the glycogen granules isolated from Gyg KO muscle were larger than those purified from WT muscle and that they extended over a wide range of sizes, reaching up to a 4-fold greater radius than the particles in the WT animal (Figure 1E). Electron microscopy studies also showed large particles, which accumulated in the intermyofibrillar space of Gyg KO muscle (Figures 1F and 1G and Figures S1F and 1G).

Glycogen Synthesis Does Not Require a Protein Primer

The presence of glycogen in the absence of glycogenin implies one of two possibilities: (1) glycogen is synthesized without a priming protein; or (2) another unknown protein replaces glycogenin in the Gyg KO mice. To address these questions, we designed a mass spectrometry-based approach to identify proteins covalently bound to the polysaccharide.

Glycogen was purified from the skeletal muscle of Gyg KO mice and control littermates by digesting the tissues with 30% KOH under conditions in which the protein that was covalently bound to glycogen were not completely hydrolyzed. The resulting glycogen samples were repeatedly washed in order to remove the non-covalently bound peptides. Glycogen samples, which retained the covalently linked peptides, were then degraded with α-amylase or amyloglucosidase (Figure S1H). These two enzymes differ in their ability to act on the covalent bond between an amino acid and a glucose residue. While amyloglucosidase cuts the covalent link (meaning that no hexose should be found in the treated peptides), amylase is not able to cut the covalent amino acid-sugar bond, meaning that all the peptides covalently bound to glycogen should still carry at least one hexose (Table S2). According to our experimental design, criteria for the identification of a glycogenin substitute in the glycogen purified from Gyg KO mice would be as follows: presence of peptide(s) originating from the primer in the samples treated with both amylase and amyloglucosidase, and at least one hexose residue in the sample treated with amylase. We identified the resulting peptides by mass spectrometry. The proteins to which they belong are listed in Table S3 and Figure 1H. As expected, in the analysis of WT samples, only glycogenin fulfilled the selection criteria (i.e., was present in the two series). Strikingly, in the glycogen extracted from skeletal muscle of Gyg KO mice, no protein corresponding to both selection criteria was identified, indicating that glycogen is synthesized without a protein primer in these animals (Table S3).

Glycogenin Depletion Alters Skeletal Muscle Functionality

To assess the consequences of glycogenin depletion on muscle performance, we subjected Gyg KO and WT mice to forced exercise on a treadmill increasing in speed, until exhaustion. A strong association between muscle glycogen levels and strenuous exercise performance has been previously described (Bergström et al., 1967; Hermansen et al., 1967). Unexpectedly, in spite of the higher glycogen level in Gyg KO muscle, these

(C) Biochemical quantification of glycogen content in skeletal muscle, heart, liver, and brain of adult littermates. WT: n = 6; Gyg +/−: n = 5; Gyg KO: n = 6.
(D) Iodine spectra of glycogen purified from skeletal muscle (Gyg KO and WT littermates), commercial glycogen, and amylose.
(E) Size exclusion chromatography (SEC) of glycogen isolated from mouse skeletal muscle. The x axis represents the radius of the glycogen particles.
(F) Electron microscopy of purified glycogen particles from the quadriceps of WT and Gyg KO mice. Top panel scale bar: 200 nm; bottom panel scale bar: 100 nm.
(G) Electron microscopy of quadriceps muscle isolated from control and Gyg KO mice. Scale bar: 500 nm.
(H) Venn diagram reporting the number of proteins detected by mass spectrometry in each subgroup of the analyzed samples of glycogen purified from skeletal muscle (WT and Gyg KO), treated with α-amylase or amyloglucosidase.
All studies have been conducted in control and Gyg KO mice between 15 and 20 weeks of age, unless otherwise indicated. Data are expressed as mean ± SEM. *p < 0.05; **p < 0.01; ***p < 0.001. See also Figure S1.

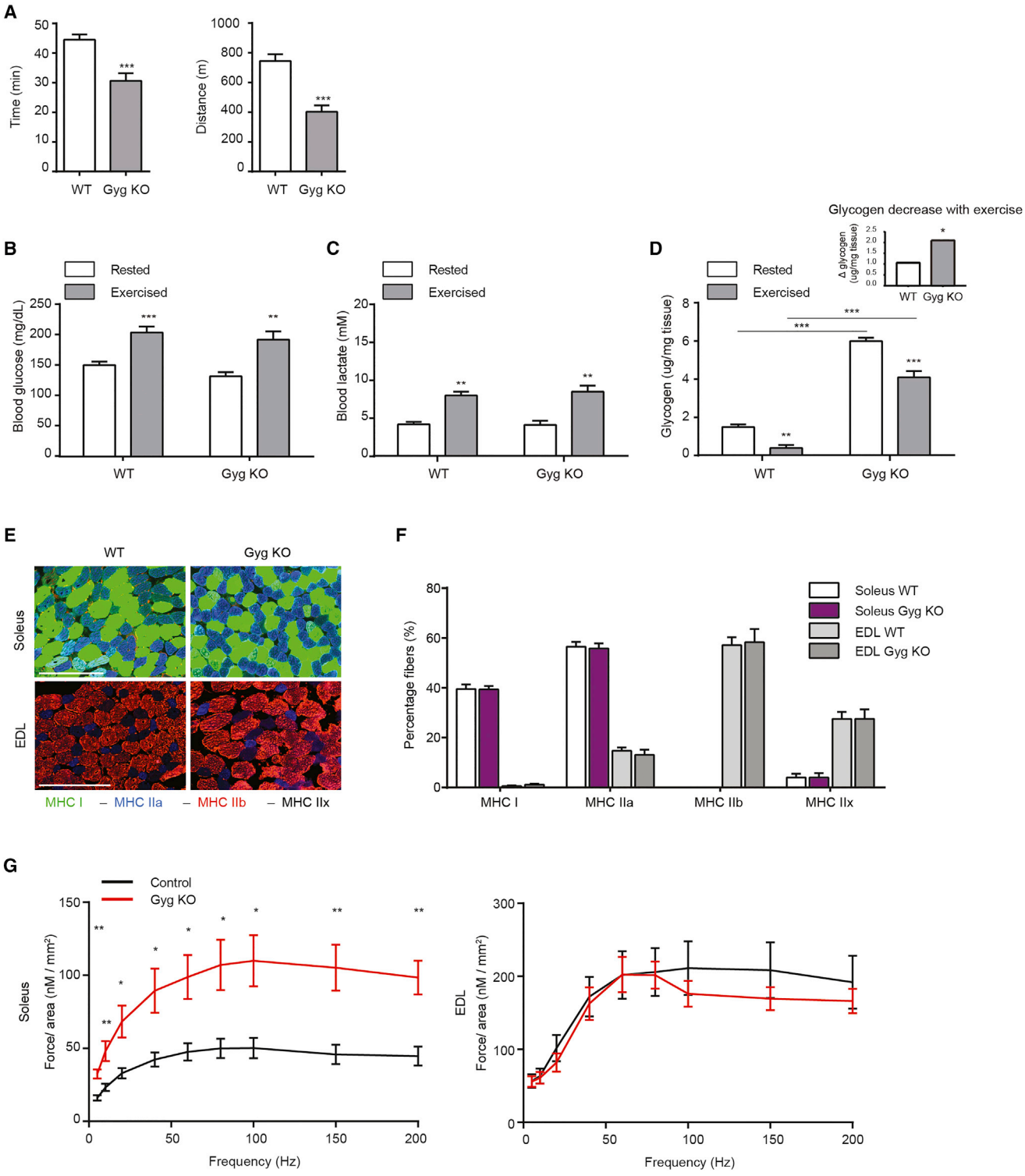

Figure 2. Gyg Depletion Impairs Skeletal Muscle Functionality

(A) Running time and distance were measured from the individual performances on the treadmill. WT: n = 9; Gyg KO: n = 8.

(B) Glycemia was measured just before and after treadmill exercise. Statistical analyses were performed in R using the Wilcoxon/Mann-Whitney U test (non-parametric analog for two-sample t test) to compare variables of interest between WT and KO groups. WT: n = 9; Gyg KO: n = 8.

(C) Blood lactate was measured just before and after treadmill exercise. Statistical analyses were performed in R using the Wilcoxon/Mann-Whitney U test (non-parametric analog for two-sample t test) to compare variables of interest between WT and KO groups. WT: = 9; Gyg KO: = 8.

(legend continued on next page)

animals reached exhaustion earlier and covered a shorter distance compared to WT animals (Figure 2A and Figures S2A and S2B).

Both groups showed a comparable increase in blood glucose and lactate levels at exhaustion (Figures 2B and 2C). Although higher levels of glycogen remained in the muscles of Gyg KO mice at exhaustion, skeletal muscle glycogen diminished in both control and Gyg KO mice upon exercise, indicating that the poorer exercise performance in Gyg KO mice is not due to an impaired ability to mobilize glycogen (Figure 2D). In fact, the consumption of this polysaccharide was almost 2-fold higher in Gyg KO than in WT animals (Figure 2D, insert). This suggests an overall glycolytic shift in muscle metabolism.

We next carried out *ex vivo* testing of the mechanical properties of isolated muscles representative of the two opposing metabolic and contractile types. Specifically, we tested the slow-twitch soleus muscle (rich in type I fibers, which use oxidative metabolism and serve to cover prolonged resistance activity) and fast-twitch EDL muscle (rich in type II glycolytic fibers, which use anaerobic metabolism and serve to sustain short, high-intensity activity). First, we verified that the muscle mass was maintained and that both soleus and EDL had increased glycogen in the Gyg KO model (Figures S2C and S2D). We also ruled out the existence of alterations in the proportion of fiber types in soleus and EDL by immunohistochemical analyses with antibodies specific for myosin heavy chain (MHC) I, IIa, and IIb (MHC IIX were quantified by exclusion of positive staining) (Figures 2E and 2F).

Isometric force generation after applying trains of stimuli at increasing frequency (Figure 2G) was recorded in Gyg KO and control muscles. Remarkably, Gyg KO soleus generated a force approximately 2-fold greater than its paired WT control at all the stimulation frequencies tested, while Gyg KO EDL responded with a force comparable to that of control littermates. These results suggest that glycogen accumulation in the absence of glycogenin specifically modifies the performance of the oxidative soleus toward a more glycolytic type, while no significant effect occurs in muscles with a pre-existing glycolytic metabolism, such as the EDL.

Glycogenin-Depleted Animals Show Changes in Muscle Oxidative Metabolism

We next tested the energy expenditure of the two genotypes in a resting condition by measuring V_{O2} and V_{CO2} (Figure 3A and Figure S3A). Indirect calorimetric measurements indicated lower energy consumption in adult Gyg KO animals. Oxygen consumption was lower over the whole day and was associated with a reduction in glucose oxidation (prominent in the dark phase when mice are awake and more active) and diminished lipid oxidation (especially during the light phase when mice are asleep). We confirmed that the differences observed were not due to anomalies in body weight or the proportion of fat:lean body mass, which were both found to be equally maintained in the two animal models (Figures S3B and S3C). Moreover, food intake and locomotor activity were comparable (Figures S3A and S3D).

To further characterize the metabolism in the two muscles, we measured mitochondrial respiration using high-resolution respirometry in isolated soleus and EDL. Once again, we identified a change in the soleus of Gyg KO mice, which showed lower oxygen consumption affecting all mitochondrial states. These lower levels were comparable to those of fast-twitch muscles (e.g., WT EDL). On the other hand, EDL respiration values were not altered in the Gyg KO, giving oxygen consumption values comparable to those of control muscle (Figure 3B). However, the differences observed in the Gyg KO soleus were not due to a decreased number of mitochondria (Figures 3C and 3D) or to a specific decrease in OXPHOS proteins (Figures 3E and 3F and Figure S3E). We then quantified the adenylate energy charge in the two muscles. No differences were found for EDL, while Gyg KO soleus presented with lower AMP/ATP and ADP/ATP ratios than WT soleus, approaching those found in the EDL (Figure 3E).

Forced Over-accumulation of Glycogen in Skeletal Muscle Recapitulates the Changes Observed in the Glycogenin-Deficient Muscles

The alterations observed in the Gyg KO mouse model could be a result of the absence of glycogenin or the increased accumulation of glycogen in muscles. To discern between the two possibilities, we generated an animal model with skeletal muscle-specific expression of a form of MGS that cannot be inactivated by phosphorylation (9A-MGS^{MLC1}) (Figure 4A). In resting conditions, these animals accumulated 7-fold more glycogen in this tissue compared to their WT littermates (Figure 4B). PAS staining of muscle sections showed that glycogen was uniformly distributed and was mostly degradable by amylase treatment (Figure 4C). Interestingly, western blot analyses showed an increase in the quantity of glycogenin, paralleling that of glycogen. To explore whether this increased muscle glycogen affects exercise performance, we subjected mice to forced exercise on a treadmill. 9A-MGS^{MLC1} mice reached exhaustion faster than their control littermates, despite the observed mobilization of muscle glycogen during exercise (Figure 4D). Indeed, as seen in Gyg KO

(D) Biochemical measurement of glycogen content in skeletal muscle from mice in resting condition and mice at the point of exhaustion immediately following the treadmill experiment. The insert figure (top right panel) indicates the decrease in glycogen after exercise. p values for the differences between glycogen values for genotype/exercise groups and for their interaction were calculated using a general linear model. n = 6.

(E) Cross-sections of soleus and EDL muscle were stained for fiber type differentiation using antibodies against MHCs. All staining was performed on frozen sections. Scale bar: 250 μm.

(F) Relative proportions of muscle fiber types in the soleus and EDL muscle of WT and Gyg KO mice from MHC stained sections. SOL: WT: n = 7; Gyg KO: n = 13. EDL: WT: n = 9; Gyg KO: n = 7.

(G) *Ex vivo* force-frequency curve generated by incremental stimulation frequency normalized for muscle area of the soleus and EDL. SOL: WT: n = 5; Gyg KO: n = 4. EDL: WT: n = 5; Gyg KO: n = 5.

All studies have been conducted in control and Gyg KO mice between 15 and 20 weeks of age, unless otherwise indicated. Data are expressed as mean ± SEM. *p < 0.05; **p < 0.01; ***p < 0.001. See also Figure S2.

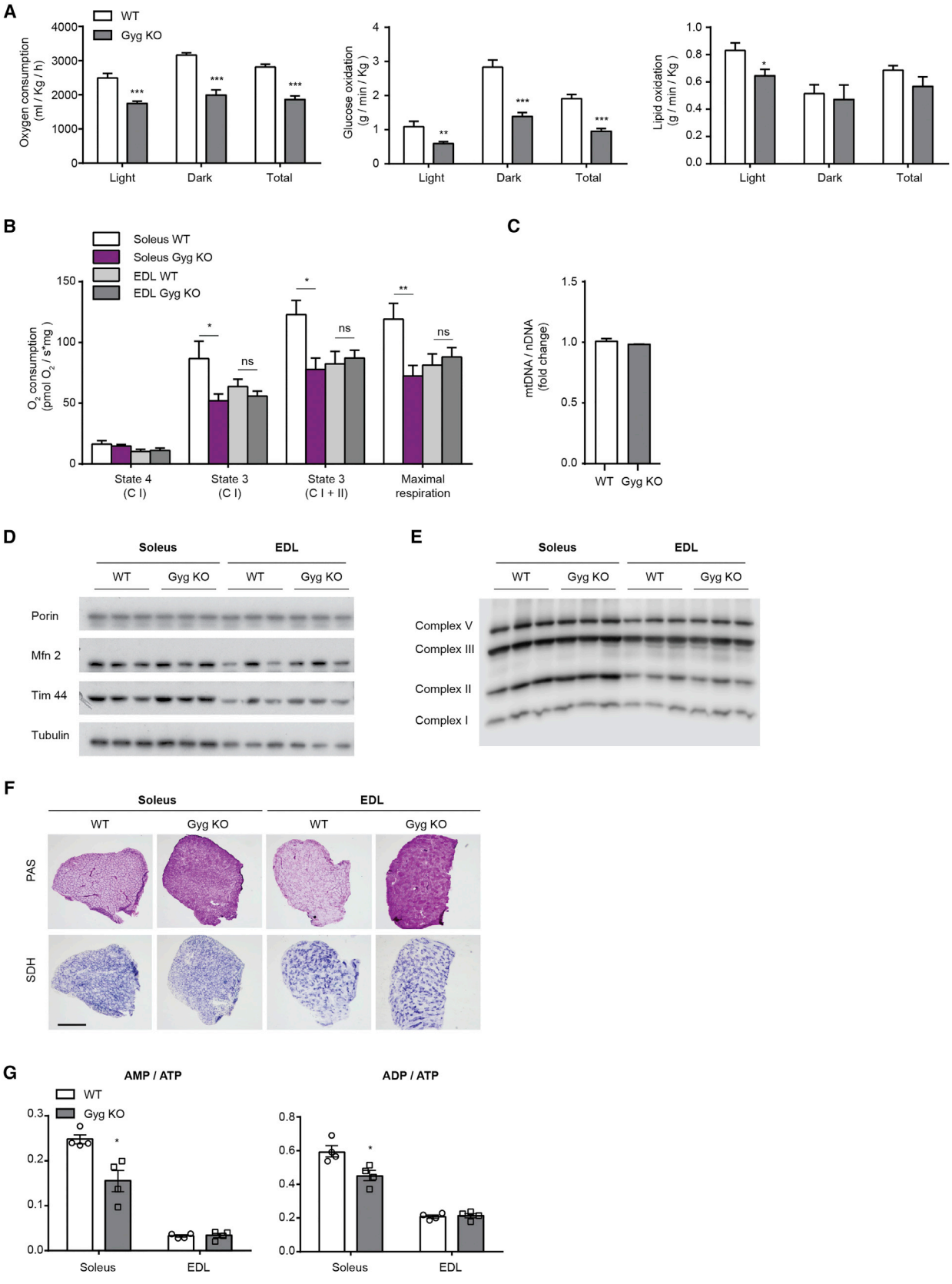

(legend on next page)

mice, the net quantity of glycogen degraded after exercise was higher in 9A-MGS^{MLC1} animals than in controls (Figure 4B). We next analyzed mitochondrial respiration in fibers extracted from soleus and EDL muscles of 9A-MGS^{MLC1} mice. As in the Gyg KO animal, the soleus of 9A-MGS^{MLC1} mice showed reduced mitochondrial respiration compared to control littermates (Figure 4E). Taken together, the results from the 9A-MGS^{MLC1} mice are consistent with the changes observed in the Gyg KO animals and suggest that the over-accumulation of glycogen (rather than the absence of glycogenin) is the underlying cause of the glycolytic switch in oxidative muscles.

DISCUSSION

Our results unveil new and unexpected aspects of glycogen metabolism and challenge the concept that glycogenin is indispensable for glycogen synthesis (Zeqiraj et al., 2014). In addition to showing that glycogen is efficiently synthesized in animals lacking glycogenin, we further demonstrate that a priming protein is unnecessary for the synthesis of this polysaccharide. Furthermore, the finding that the striated muscles of Gyg KO mice display an over-accumulation of glycogen suggests that glycogenin depletion leads to a situation that is exactly the opposite of that expected.

One of our most striking findings is that glycogen synthesis in Gyg KO mice proceeds without a priming protein. In fact, this phenomenon can be seen in other organisms, such as bacteria, yeast, and plants (Szydlowski et al., 2009; Torija et al., 2005; Ugalde et al., 2003), in which GS homologs act as *de novo* initiators. Our hypothesis is that glycogen is synthesized by GS in Gyg KO animals, starting from free glucose. In support of this, Salsas and Larner demonstrated that, in the presence of UDP-glucose as a co-substrate, purified muscle GS converts glucose to maltose (Salsas and Larner, 1975). Other authors showed that GS can convert maltose into maltotriose (Goldemberg, 1962) and that the reaction may subsequently proceed to form oligosaccharides with an increasing number of glucose residues, with the Km decreasing progressively alongside the length of the acceptor chain (Larner et al., 1976).

Unlike the glycogen aggregates seen to accumulate in Lafora disease (Duran et al., 2014; Duran and Guinovart, 2015), the glycogen synthesized by the murine Gyg KO model did not form aggregates, demonstrated a regular degree of branching, and was hydrolyzed *in vitro* by amylase treatment. The latter is in accordance with it being metabolically active *in vivo* and degraded, at least in part, during exercise. Remarkably, glycogen particles from Gyg KO animals were larger than those from controls, as measured by chromatography and EM. The observation that Gyg KO muscle contains a higher quantity of glycogen than that of the WT control indicates that glycogenin may act as a regulator of glycogen content. There are various possible rationales for this. First, it is known that GS and Gyg interact strongly; therefore, glycogenin may modulate the amount of glycogen synthesized by acting on GS (Skurat et al., 2006). This idea is supported by our observation that the skeletal muscle and heart of Gyg heterozygous mice, which have reduced glycogenin expression, also accumulate more glycogen than WT animals. Second, Gyg could be important for the regulation of glycogen particle size, limiting the final volume of the particle. In favor of this hypothesis is our observation that the particles in Gyg KO muscle were larger than those present in WT animals. Furthermore, glycogenin overexpression in rat fibroblasts leads to a greater number of smaller molecules, rather than increasing glycogen production (Skurat et al., 1997).

In contrast to the prediction that glycogen accumulation in Gyg KO mice would confer greater resistance to fatigue (Bergström et al., 1967; Holloszy and Kohrt, 1996; Karlsson and Saltin, 1971), these animals reached exhaustion faster than controls when challenged with strenuous exercise. Importantly, simply generating an over-accumulation of glycogen in the muscle of 9A-MGS^{MLC1} mice caused a similar defect in muscle performance, consistent with the observation in absence of glycogenin. Although we cannot rule out the different glycogen particle size as a cause of the reduced exercise resistance in the Gyg KO model, the recapitulation of this phenotype in 9A-MGS^{MLC1} animals supports the key role of glycogen accumulation in the regulation of muscle function.

Our results also support the idea that the greater availability of glycogen in the muscles of both Gyg KO and 9A-MGS^{MLC1} mice induces oxidative fibers to preferentially use this polysaccharide. This renders them more glycolytic, similar to bona fide type II glycolytic fibers, which primarily use glycogen as a fuel. The aforementioned metabolic switch occurs despite the absence of changes in fiber type proportions (as revealed by MHC analysis) or levels of mitochondrial markers (such as porin, mitofusin 2, Tim44, OXPHOS proteins, and succinate dehydrogenase activity: demonstrated by SDH staining). Nevertheless, Gyg KO animals display lower energy expenditure and low oxygen consumption in a steady rested state, indicating a lower glucose and lipid oxidation capacity. Indeed, significant changes in mitochondrial respiration indicative of impaired functionality were detected by measuring oxygen consumption in permeabilized

Figure 3. Glycogenin Deficiency Affects Oxidative Metabolism

(A) Calorimetric parameters were obtained from metabolic cages in Gyg KO and WT animals. O_2 consumption, glucose oxidation, and lipid oxidation were measured during the light phase, dark phase, and overall. n = 7.

(B) Mitochondrial respiration indicated by oxygen consumption during different OXPHOS stages in soleus and EDL muscle. n = 11.

(C) Mitochondrial content assessed by mtDNA copy number in soleus. WT n = 5; Gyg KO n = 6.

(D) Immunoblot for mitochondrial proteins from soleus and EDL muscle extracted from Gyg KO and WT adult males. Porin, Mfn2, and Tim 44. Tubulin was used as a loading control.

(E) Protein expression of the subunits of respiratory chain complexes in soleus and EDL muscle (Complex I: NDUFB8; Complex II: SDHB; Complex III: UQCR2; Complex V: ATP5A).

(F) PAS and SDH staining in parallel sections of OCT-embedded soleus and EDL muscle of WT and Gyg KO adult males. SDH is used as a mitochondrial marker.

(G) Measure of adenylated nucleotide ratios: AMP/ATP and ADP/ATP in the soleus and EDL muscles of adult Gyg KO and WT males. n = 4.

All studies have been conducted in control and Gyg KO mice between 15 and 20 weeks of age, unless otherwise indicated. Data are expressed as mean ± SEM. *p < 0.05; **p < 0.01; ***p < 0.001. See also Figure S3.

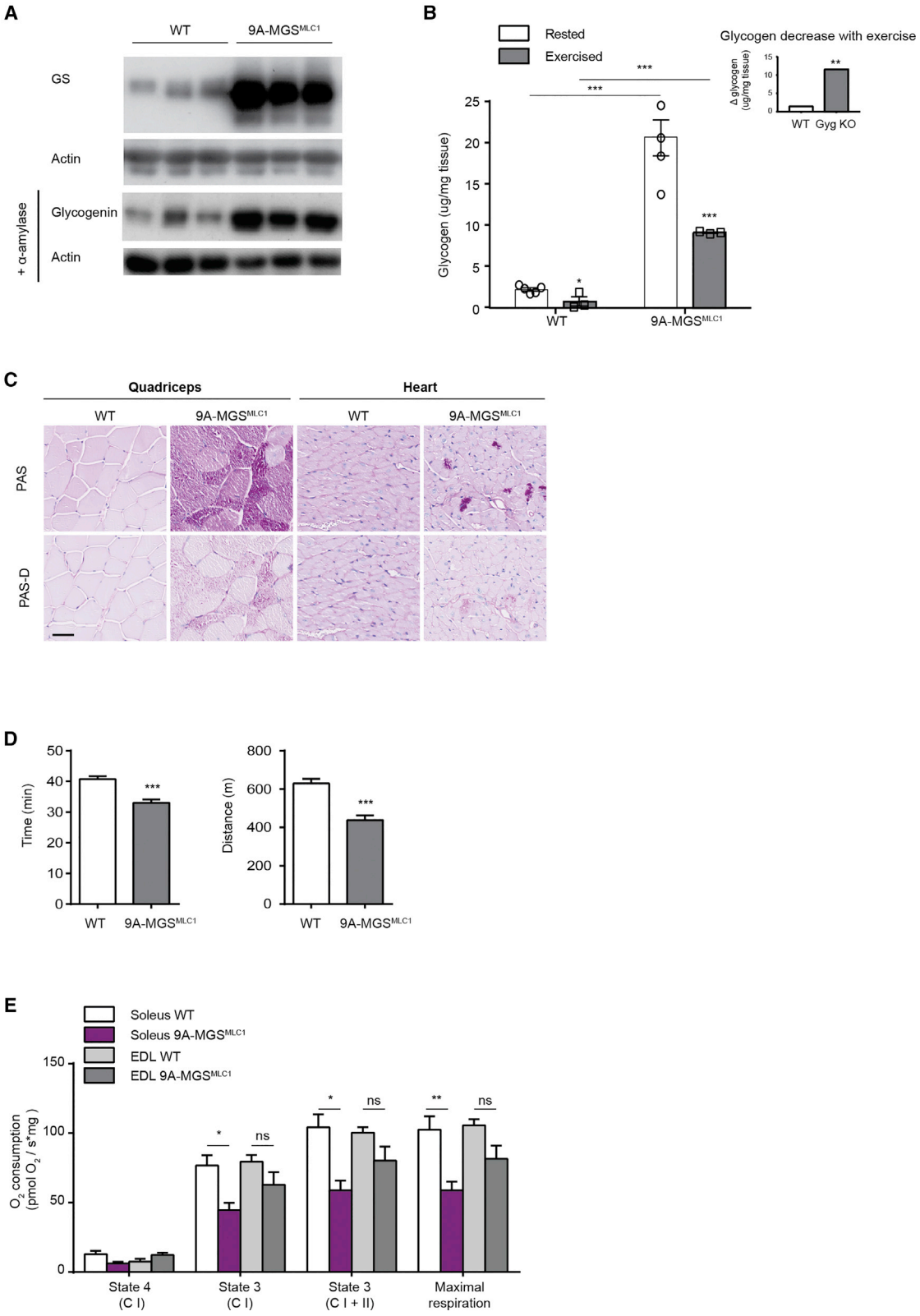

Figure 4. Muscle Glycogen Over-accumulation Causes Skeletal Muscle Energetic Impairment

(A) Western blot characterization of the 9A-MGS^{MLC1} mouse model: GS was detected in total tissue homogenate from skeletal muscle; loading control β-actin. Glycogenin was detected in α-amylase-treated samples from total homogenate of skeletal muscle; loading control β-actin.

(legend continued on next page)

muscle fibers from the soleus. Our current hypothesis is that the high availability of glycogen in Gyg KO soleus muscle affects energy production, impairing oxidative metabolism. This type of metabolism is particularly important when energy demands are high, such as during endurance exercise. In contrast, the high glycogen content found in the EDL muscle of this mouse model does not lead to any changes in metabolism, likely because these fibers normally utilize glycogen as their main energy source. Thus, a high degree of glycogen accumulation leads to an alteration of muscle function and oxygen consumption in a muscle that is predominantly reliant on oxidative metabolism. This translates into low resistance during prolonged, low-intensity activity.

Despite the high availability of degradable glycogen, both the Gyg KO and 9A-MGS^{MLC1} models showed a similar, low resistance to fatigue when forced to exercise on a treadmill until exhaustion. An alteration in mitochondrial respiration was also found in the 9A-MGS^{MLC1} mice, which may explain the poor endurance performance. On the basis of our findings, we conclude that the high glycogen content in the muscles of Gyg KO and 9A-MGS^{MLC1} mice decreases muscle endurance, against all expectations.

Humans and most mammals carry two isoforms of the glycogenin gene, namely GYG1 and GYG2. GSD XV is a recently described rare human disease caused by GYG1 depletion. As mice express only Gyg1, the Gyg KO mouse constitutively lacks the protein throughout the body. Comparison of GSD XV with Gyg KO mice is therefore beneficial to provide new insights into the role of glycogenin and the physiopathology of GSD XV. Like these patients (Akman et al., 2016; Colombo et al., 2016; Luo et al., 2015; Malfatti et al., 2014), Gyg KO animals also accumulate glycogen in skeletal muscle and show phenotypical muscle weakness. However, while the glycogen in Gyg KO mice is entirely amylase sensitive, the glycogen that accumulates in GSD XV patients is accompanied by polyglucosans. This may contribute to the more severe muscle weakness phenotype in humans. Moreover, the Gyg KO model also shows glycogen accumulation in the heart. This may be of special interest regarding GSD XV patients, some of whom have been shown to suffer from cardiomyopathy and require a heart transplant (Hedberg-Oldfors et al., 2017).

In conclusion, a lack of glycogenin does not prevent the synthesis of glycogen, but rather causes an over-accumulation of the polysaccharide in striated muscle, reflective of GSD XV patients. Although the over-accumulated glycogen can be mobilized, it leads to functional impairment and metabolic rearrangement. These observations offer a new perspective on glycogen synthesis and the role of the glycogenin-glycogen relationship in muscle physiology.

STAR★METHODS

Detailed methods are provided in the online version of this paper and include the following:

- KEY RESOURCES TABLE
- CONTACT FOR REAGENT AND RESOURCE SHARING
- EXPERIMENTAL MODEL AND SUBJECT DETAILS
  - Animals
- METHOD DETAILS
  - Histochemistry
  - Biochemical analysis
  - Glycogen particle analysis
  - Transmission electron microcopy
  - Quantitative RT-PCR
  - Metabolite determination
  - Respiration studies in permeabilized muscle
  - Indirect calorimetry
  - Food intake, body temperature and weight
  - Mass spectrometry
  - Treadmill exercise
  - Myo-mechanical analysis of isolated muscles
- QUANTIFICATION AND STATISTICAL ANALYSIS
  - Statistical Analysis
- DATA AND SOFTWARE AVAILABILITY

SUPPLEMENTAL INFORMATION

Supplemental Information includes three figure and three tables and can be found with this article online at http://dx.doi.org/10.1016/j.cmet.2017.06.008.

AUTHOR CONTRIBUTIONS

G.T. designed and performed experiments, analyzed experimental data, and participated in the manuscript preparation. J.D. and M.G.-R. performed experiments and analyzed experimental data. F.V. performed the SEC analysis and contributed to the discussion of the results. A.L.S. contributed to the performances of animal experiments. D.S. helped with respiration studies and advice. I.L.-S, M.A.S., and F.S. contributed to the design of the experiments and discussion of the results. M.V. advised, assisted, and supervised mass spectrometry analysis. P.M.-C. assisted in the myograph experiment. J.J.G. designed and supervised the whole project and revised the manuscript.

ACKNOWLEDGMENTS

We wish to thank the following members of IRB Barcelona: Anna Adrover, Emma Veza, Natalia Plana, and Vanessa Hernandez for technical assistance;

(B) Biochemical measurement of glycogen content in the skeletal muscle of mice in a resting state and mice at the point of exhaustion following the treadmill experiment. The top right panel indicates the decrease in glycogen after exercise. p values for the differences between glycogen values for each genotype/exercise groups and for their interaction were calculated using a general linear model. Rested WT: n = 5; rested 9A-MGS^{MLC1}: n = 4; exercised: n = 3.
(C) Glycogen over-accumulation in skeletal muscle fibers is shown by PAS staining in quadriceps from 9A-MGS^{MLC1} mice and control mice. A minor degree of glycogen accumulation is shown in cardiac muscle, characterized by lower expression of the MLC1 gene compared to skeletal muscle. Glycogen degradability is shown by PAS-D staining in serial tissue slices embedded in paraffin. Scale bar: 25 μm.
(D) Resistance endurance of 9A-MGS^{MLC1} mice tested by treadmill exercise. Total exercise average is shown as exhaustion time and distance covered. n = 9.
(E) Mitochondrial respiration indicated by oxygen consumption during different OXPHOS stages in the soleus muscle of control and 9A-MGS^{MLC1} mice. WT: n = 5; 9A-MGS^{MLC1}: n = 6.
All studies have been conducted in control and Gyg KO mice between 15 and 20 weeks of age, unless otherwise indicated. Data are expressed as mean ± SEM. *p < 0.05; **p < 0.01; ***p < 0.001.

and Dr. Antonio Zorzano for essential reagents and advice, the histopathology, the mouse mutant, and the biostatistics/bioinformatics core facilities. Thanks also to Dr. Marina Gay for mass spectrometry advice and data analysis and Dr. Mireia Díaz-Lobo for mass spectrometry experiments. Mass spectrometry was performed at the IRB Barcelona Mass Spectrometry and Proteomics Core Facility, which actively participates in the BMBS European COST Action BM 1403 and is a member of Proteored, PRB2-ISCIII, supported by grant PRB2 (IPT13/0001 - ISCIII-SGEFI / FEDER). Thanks also to Dr. Carmen Lopez-Iglesias (University of Barcelona) for assistance with the electron microscope. G.T. is supported by the "La Caixa" PhD Fellowship Program. IRB Barcelona is the recipient of a Severo Ochoa Award of Excellence from MINECO (Government of Spain). This study was supported by grants from the Spanish MINECO (BFU2011-30554-C02-00 and SAF2014-54525-P). M.A.S. was supported by an NHMRC CJ Martin Fellowship (GNT1092451). NIH grants to Velocigene at Regeneron (U01HG004085) and the CSD Consortium (U01HG004080) funded the generation of gene-targeted ES cells in the KOMP Program. None of the supporting agencies had any role in establishing the work or in writing the manuscript.

Received: January 12, 2017
Revised: May 8, 2017
Accepted: June 13, 2017
Published: July 5, 2017

REFERENCES

Akman, H.O., Aykit, Y., Amuk, O.C., Malfatti, E., Romero, N.B., Maioli, M.A., Piras, R., DiMauro, S., and Marrosu, G. (2016). Late-onset polyglucosan body myopathy in five patients with a homozygous mutation in GYG1. Neuromuscul. Disord. *26*, 16–20.

Alonso, M.D., Lomako, J., Lomako, W.M., and Whelan, W.J. (1995). A new look at the biogenesis of glycogen. FASEB J. *9*, 1126–1137.

Bergström, J., Hermansen, L., Hultman, E., and Saltin, B. (1967). Diet, muscle glycogen and physical performance. Acta Physiol. Scand. *71*, 140–150.

Cao, Y., Mahrenholz, A.M., DePaoli-Roach, A.A., and Roach, P.J. (1993). Characterization of rabbit skeletal muscle glycogenin. Tyrosine 194 is essential for function. J. Biol. Chem. *268*, 14687–14693.

Chan, T.M., and Exton, J.H. (1976). A rapid method for the determination of glycogen content and radioactivity in small quantities of tissue or isolated hepatocytes. Anal. Biochem. *71*, 96–105.

Colombo, I., Pagliarani, S., Testolin, S., Cinnante, C.M., Fagiolari, G., Ciscato, P., Bordoni, A., Fortunato, F., Magri, F., Previtali, S.C., et al. (2016). Longitudinal follow-up and muscle MRI pattern of two siblings with polyglucosan body myopathy due to glycogenin-1 mutation. J. Neurol. Neurosurg. Psychiatry *87*, 797–800.

Duran, J., and Guinovart, J.J. (2015). Brain glycogen in health and disease. Mol. Aspects Med. *46*, 70–77.

Duran, J., Tevy, M.F., Garcia-Rocha, M., Calbó, J., Milán, M., and Guinovart, J.J. (2012). Deleterious effects of neuronal accumulation of glycogen in flies and mice. EMBO Mol. Med. *4*, 719–729.

Duran, J., Gruart, A., García-Rocha, M., Delgado-García, J.M., and Guinovart, J.J. (2014). Glycogen accumulation underlies neurodegeneration and autophagy impairment in Lafora disease. Hum. Mol. Genet. *23*, 3147–3156.

García-Rocha, M., Roca, A., De La Iglesia, N., Baba, O., Fernández-Novell, J.M., Ferrer, J.C., and Guinovart, J.J. (2001). Intracellular distribution of glycogen synthase and glycogen in primary cultured rat hepatocytes. Biochem. J. *357*, 17–24.

Gilboe, D.P., Larson, K.L., and Nuttall, F.Q. (1972). Radioactive method for the assay of glycogen phosphorylases. Anal. Biochem. *47*, 20–27.

Goldemberg, S.H. (1962). Specificity of uridine diphosphate glucose-glycogen glucosyltransferase. Biochim. Biophys. Acta *56*, 357–359.

Hedberg-Oldfors, C., Glamuzina, E., Ruygrok, P., Anderson, L.J., Elliott, P., Watkinson, O., Occleshaw, C., Abernathy, M., Turner, C., Kingston, N., et al. (2017). Cardiomyopathy as presenting sign of glycogenin-1 deficiency-report of three cases and review of the literature. J. Inherit. Metab. Dis. *40*, 139–149.

Hermansen, L., Hultman, E., and Saltin, B. (1967). Muscle glycogen during prolonged severe exercise. Acta Physiol. Scand. *71*, 129–139.

Holloszy, J.O., and Kohrt, W.M. (1996). Regulation of carbohydrate and fat metabolism during and after exercise. Annu. Rev. Nutr. *16*, 121–138.

Karlsson, J., and Saltin, B. (1971). Diet, muscle glycogen, and endurance performance. J. Appl. Physiol. *31*, 203–206.

Krisman, C.R., and Barengo, R. (1975). A precursor of glycogen biosynthesis: alpha-1,4-glucan-protein. Eur. J. Biochem. *52*, 117–123.

Larner, J., Takeda, Y., and Hizukuri, S. (1976). The influence of chain size and molecular weight on the kinetic constants for the span glucose to polysaccharide for rabbit muscle glycogen synthase. Mol. Cell. Biochem. *12*, 131–136.

López-Soldado, I., Zafra, D., Duran, J., Adrover, A., Calbó, J., and Guinovart, J.J. (2015). Liver glycogen reduces food intake and attenuates obesity in a high-fat diet-fed mouse model. Diabetes *64*, 796–807.

Luo, S., Zhu, W., Yue, D., Lin, J., Wang, Y., Zhu, Z., Qiu, W., Lu, J., Hedberg-Oldfors, C., Oldfors, A., and Zhao, C. (2015). Muscle pathology and whole-body MRI in a polyglucosan myopathy associated with a novel glycogenin-1 mutation. Neuromuscul. Disord. *25*, 780–785.

Malfatti, E., Nilsson, J., Hedberg-Oldfors, C., Hernandez-Lain, A., Michel, F., Dominguez-Gonzalez, C., Viennet, G., Akman, H.O., Kornblum, C., Van den Bergh, P., et al. (2014). A new muscle glycogen storage disease associated with glycogenin-1 deficiency. Ann. Neurol. *76*, 891–898.

Mu, J., Skurat, A.V., and Roach, P.J. (1997). Glycogenin-2, a novel self-glucosylating protein involved in liver glycogen biosynthesis. J. Biol. Chem. *272*, 27589–27597.

Pessina, P., Cabrera, D., Morales, M.G., Riquelme, C.A., Gutiérrez, J., Serrano, A.L., Brandan, E., and Muñoz-Cánoves, P. (2014). Novel and optimized strategies for inducing fibrosis in vivo: focus on Duchenne Muscular Dystrophy. Skelet. Muscle *4*, 7.

Sala, D., Ivanova, S., Plana, N., Ribas, V., Duran, J., Bach, D., Turkseven, S., Laville, M., Vidal, H., Karczewska-Kupczewska, M., et al. (2014). Autophagy-regulating TP53INP2 mediates muscle wasting and is repressed in diabetes. J. Clin. Invest. *124*, 1914–1927.

Salsas, E., and Larner, J. (1975). Glycogen synthase can use glucose as an acceptor. J. Biol. Chem. *250*, 1833–1837.

Schiaffino, S., and Reggiani, C. (1996). Molecular diversity of myofibrillar proteins: gene regulation and functional significance. Physiol. Rev. *76*, 371–423.

Sebastián, D., Sorianello, E., Segalés, J., Irazoki, A., Ruiz-Bonilla, V., Sala, D., Planet, E., Berenguer-Llergo, A., Muñoz, J.P., Sánchez-Feutrie, M., et al. (2016). Mfn2 deficiency links age-related sarcopenia and impaired autophagy to activation of an adaptive mitophagy pathway. EMBO J. *35*, 1677–1693.

Skurat, A.V., Lim, S.S., and Roach, P.J. (1997). Glycogen biogenesis in rat 1 fibroblasts expressing rabbit muscle glycogenin. Eur. J. Biochem. *245*, 147–155.

Skurat, A.V., Dietrich, A.D., and Roach, P.J. (2006). Interaction between glycogenin and glycogen synthase. Arch. Biochem. Biophys. *456*, 93–97.

Smythe, C., and Cohen, P. (1991). The discovery of glycogenin and the priming mechanism for glycogen biogenesis. Eur. J. Biochem. *200*, 625–631.

Sullivan, M.A., Powell, P.O., Witt, T., Vilaplana, F., Roura, E., and Gilbert, R.G. (2014). Improving size-exclusion chromatography separation for glycogen. J. Chromatogr. A *1332*, 21–29.

Szydlowski, N., Ragel, P., Raynaud, S., Lucas, M.M., Roldán, I., Montero, M., Muñoz, F.J., Ovecka, M., Bahaji, A., Planchot, V., et al. (2009). Starch granule initiation in Arabidopsis requires the presence of either class IV or class III starch synthases. Plant Cell *21*, 2443–2457.

Thomas, J.A., Schlender, K.K., and Larner, J. (1968). A rapid filter paper assay for UDPglucose-glycogen glucosyltransferase, including an improved biosynthesis of UDP-14C-glucose. Anal. Biochem. *25*, 486–499.

Torija, M.J., Novo, M., Lemassu, A., Wilson, W., Roach, P.J., François, J., and Parrou, J.L. (2005). Glycogen synthesis in the absence of glycogenin in the yeast Saccharomyces cerevisiae. FEBS Lett. *579*, 3999–4004.

Ugalde, J.E., Parodi, A.J., and Ugalde, R.A. (2003). De novo synthesis of bacterial glycogen: Agrobacterium tumefaciens glycogen synthase is involved

in glucan initiation and elongation. Proc. Natl. Acad. Sci. USA *100*, 10659–10663.

Vizcaíno, J.A., Csordas, A., Del-Toro, N., Dianes, J.A., Griss, J., Lavidas, I., Mayer, G., Perez-Riverol, Y., Reisinger, F., Ternent, T., et al. (2016). 2016 update of the PRIDE database and its related tools. Nucleic Acids Res. *44*, 11033.

Whelan, W.J. (1986). The initiation of glycogen synthesis. BioEssays *5*, 136–140.

Zeqiraj, E., Tang, X., Hunter, R.W., García-Rocha, M., Judd, A., Deak, M., von Wilamowitz-Moellendorff, A., Kurinov, I., Guinovart, J.J., Tyers, M., et al. (2014). Structural basis for the recruitment of glycogen synthase by glycogenin. Proc. Natl. Acad. Sci. USA *111*, E2831–E2840.

Zhai, L., Schroeder, J., Skurat, A.V., and Roach, P.J. (2001). Do rodents have a gene encoding glycogenin-2, the liver isoform of the self-glucosylating initiator of glycogen synthesis? IUBMB Life *51*, 87–91.

STAR★METHODS

KEY RESOURCES TABLE

REAGENT or RESOURCE	SOURCE	IDENTIFIER
Antibodies		
Mouse monoclonal anti-glycogenin (3B5):GN	Novus Biological	Cat# H00002992-M07, RRID: AB_539428
Rabbit monoclonal anti- glycogen synthase(15B1): GS	Cell Signaling Technology	Cat# 3886, RRID: AB_2116392
Mouse monoclonal anti-GAPDH (6C5)	Thermo Fisher Scientific	Cat# AM4300, RRID: AB_2536381
Rabbit polyclonal anti- VDAC1 / Porin - Mitochondrial Loading Control	Abcam	Cat# ab15895, RRID: AB_2214787
Mouse monoclonal anti-mitofusin 2: Mfn2	Abcam	Cat# ab56889, RRID: AB_2142629
Mouse monoclonal anti-Tim44 (clone 24)	BD Biosciences	Cat# 612582, RRID: AB_399869
Mouse monoclonal anti-Tubulin (clone DM1A)	Sigma-Aldrich	Cat# T9026, RRID: AB_477593
5 mouse monoclonal antibodies: Total OXPHOS Rodent WB Antibody Cocktail	Abcam	Cat# ab110413, RRID: AB_2629281
Mouse monoclonal anti-Actin (clone AC-40)	Sigma-Aldrich	Cat# A3853, RRID: AB_262137
Guinea-pig polyclonal anti- muscle glycogen phosphorylase (peptide 826-841): GP	Eurogentec	N/A
Mouse monoclonal anti-MHC Type I:BA-F8	DSHB	Cat# BA-F8 RRID: AB_10572253
Mouse monoclonal anti-MHC Type IIa: SC-71	DSHB	Cat# SC-71 RRID: AB_2147165
Mouse monoclonal anti-MHC Type IIb: BF-F3	DSHB	Cat# BF-F3, RRID: AB_2266724
Chemicals, Peptides, and Recombinant Proteins		
PAS (Artisan Periodic Acid Schiff Stain Kit)	DAKO	Cat#AR165
α-amylase	Sigma-Aldrich	Cat#A0521
REVERT Total Protein Stain	LI-COR	Cat#926-11010
glycogen type III from rabbit liver	Sigma-Aldrich	Cat#G8876
Amylose from corn	Sigma-Aldrich	Cat#A7043
Critical Commercial Assays		
RNeasy Mini kit	QIAGEN	Cat#74104
Superscript one step TM RT-PCR System	Invitrogen	Cat# 10928018
DNeasy Blood and Tissue Kit	QIAGEN	Cat# 69504
ABX Pentra Lactic Acid	HORIBA ABX	Cat# A11A01721
Deposited Data		
Mass spectrometry proteomics data	This paper	ProteomeXchange Project accession: PXD006377
Experimental Models: Organisms/Strains		
Mouse: Gyg $^{tm1a\ Wtsi}$ (C57BL/6)	KOMP	RRID: IMSR_KOMP:CSD28428-1a-Wtsi
Oligonucleotides		
Primers for RT-PCR, see Table S1	This paper	N/A
Software and Algorithms		
Proteome Discoverer software v1.4	Thermo Scientific	RRID: SCR_014477
Graphpad prism v7.00	GraphPad	RRID: SCR_002798

CONTACT FOR REAGENT AND RESOURCE SHARING

Further information and requests for resources and reagents should be directed to and will be fulfilled by the Lead Contact, Joan J. Guinovart (guinovart@irbbarcelona.org), following an approval MTA between IRB Barcelona and the receiving institution.

EXPERIMENTAL MODEL AND SUBJECT DETAILS

Animals

ES cells ($Gyg^{tm1a(KOMP)Wtsi}$) were generated by the trans-NIH Knock-Out Mouse Project (KOMP) and obtained from the KOMP Repository (www.komp.org). From ES cells, mice heterozygous for the glycogenin (Gyg) gene were generated (C57BL/6 background) and crossed to obtain Gyg KO animals. We also generated an mMGS-9A mouse model, as described in (Duran et al., 2012), and crossed it with the conditional transgenic strain MLC1-Cre (under the promoter of Myosin Light Chain 1) (Sala et al., 2014) to produce 9A-MGS^{MLC1} mice, which express MGS that cannot be inactivated in skeletal muscle. Mice were maintained in the PCB-PRBB Animal Facility Alliance under a light–dark cycle (12 hr) and specific pathogen-free conditions, with access to food and water *ad libitum*. For experimental convenience, the animals analyzed were adult males (15-20 weeks old), unless otherwise stated. All procedures were approved by the PCB Animal Experimentation Committee, in accordance with National Institutes of Health and the European Community Council Directive guidelines for the care and use of laboratory animals. Experiments were conducted using littermates. Where necessary, experimental groups included multiple litters for statistical power.

METHOD DETAILS

Histochemistry

Histochemical analyses were carried out for PAS and PAS-D using an Artisanlink Pro machine (DAKO AR165 kit). SDH staining was performed manually in a pH 7.2-7.6 solution containing Nitroblue tetrazolium (Sigma-Aldrich). Soleus and EDL fiber types were characterized by MHC immunostaining using primary monoclonal antibodies against type I (BA-F8), IIa (SC-71), and IIb (BF-F3) from the Developmental Studies Hybridoma Bank (DSHB). The secondary antibodies used were Alexa Fluor 488 goat anti-mouse IgG2b, Alexa Fluor 350 goat anti-mouse IgG1 (Invitrogen) and TRITC goat anti-mouse IgM (Millipore), respectively. Negative control slides with omission of the primary antibody were included in each immunostaining. Tissues were fixed in 4% PFA or OCT blocks in 2-methylbutane maintained in liquid nitrogen. Embedded tissues were cut into 3-μm sections. All histochemical analyses were performed successfully on a minimum of 6 animals per group, and blinded muscle fiber type counts performed.

Biochemical analysis

Tissues extracted for biochemical analysis were snap-frozen in liquid nitrogen and stored at −80°C until use. Enzymatic activity and western blot (WB) analyses were performed in frozen, pulverized tissues, which were homogenized at 4°C using a Polytron in 10 volumes of the homogenization buffer (10 mM Tris–HCl [pH 7], 150 mM KF, 15 mM EDTA, 15 mM 2-mercaptoethanol, 0.6 M sucrose, 25 nM okadaic acid, 1 mM sodium orthovanadate, 10 μg/mLleupeptin, 10 μg/mL aprotinin, 10 μg/ml pepstatin, 1 mM benzamidine, and 1 mM phenylmethanesulfonyl fluoride). Total GS activity was measured by measuring the incorporation of [U-^{14}C] glucose from UDP-[U-^{14}C] glucose into glycogen in the presence of 6.6 mmol/L of glucose-6-phosphate (G-6P) (Thomas et al., 1968). GP activity was determined by measuring the incorporation of [U-^{14}C] glucose from [U-^{14}C] glucose-1-phosphate into glycogen in the presence of 5 mmol/L AMP (Gilboe et al., 1972). Glycogenin determination was performed by western blots of homogenates treated with 13.2 U of α-amylase (A0521 from Sigma-Aldrich) per mg tissue, for 1 hr at 37°C. Western blots for mitochondrial proteins were performed in soleus and EDL muscle, homogenized using the following lysis buffer: 50 mM Tris-HCl (pH 7.4), 150 mM NaCl, 1 mM EDTA, 5 mM sodium pyrophosphate, 1 mM sodium orthovanadate, 50 mM NaF, 1% NP-40, 1 mM PMSF and a protease inhibitor mixture tablet (Roche). Homogenates were rotated for 1 hr at 4°C in an orbital shaker and centrifuged at 16,000 × *g* for 15 min at 4°C. Proteins were resolved in 10% or 15% acrylamide gels for SDS-PAGE and transferred to Immobilon membranes (Millipore). The following antibodies were used: glycogenin (clone 3B5 from Novus Biological); GS (ref. 3886 from Cell Signaling); glyceraldehyde-3-phosphate dehydrogenase (GAPDH; ref. AM4300 from Thermo Fisher Scientific); GP (polyclonal antibody generated against the peptide 826-841of muscle isoform of GP by Eurogentec, Cologne, Germany); porin (ab15895 from Abcam); Mfn2 (ref. 56889 from Abcam); mitochondrial import inner membrane translocase subunit TIM44 (ref. 612582 from BD Transduction Laboratories); Total OXPHOS Rodent Cocktail (ab110413 from Abcam); tubulin (clone DM1A from Sigma); and actin (clone AC-40 from Sigma). Proteins were detected by the ECL method (Immobilon Western Chemiluminescent HRP Substrate, Millipore). All protein detections were successfully performed on a minimum of 10 animals per group. Where otherwise specified, loading control of the WB membrane was performed using the REVERT total protein stain. Glycogen quantification was determined as previously described (García-Rocha et al., 2001). Briefly, frozen tissue was homogenized in 4 volumes of 30% KOH at 4°C. Samples were heated at 100°C for 15 min and then precipitated on a 31ET paper (Whatman, Maidstone). After three washes with 66% EtOH, dried papers were incubated with amyloglucosidase (25 U/L Sigma) in 100 mM sodium acetate buffer at pH 4.8. Glucose content was determined by the reaction with hexokinase and G-6P dehydrogenase following the original method described by Chan (Chan and Exton, 1976). Results are expressed in μg of glycogen per mg of tissue.

Glycogen particle analysis

To determine the degree of glycogen branching, skeletal muscle was homogenized in 30% KOH, heated at 100°C for 15 min, and then precipitated in 66% EtOH (v/v). Dried, purified glycogen was re-suspended in NH_4Cl (sat) plus H_2O in a 1:2 ratio, and added to the iodine-iodide solution (1.5 M KI and 100 mM I_2). Reference spectra were determined using glycogen type III from rabbit liver (Sigma G8876) and amylose (Sigma-Aldrich A7043). The absorbance spectrum was recorded from 400 to 650 nm.

SEC analysis was performed in skeletal muscle glycogen. Glycogen was obtained by KOH 30% treatment of the tissue followed by precipitation at 66% EtOH at −20°C and centrifugation at 16,000 × *g* at 4°C. The resulting pellet was re-suspended in H_2O and freeze-dried. SEC was performed as previously described (Sullivan et al., 2014).

Transmission electron microcopy

Animals were perfused and tissues were fixed with 2.5% glutaraldehyde and 2% paraformaldehyde in 0.1 M phosphate buffer. Tissue slices were post-fixed in 1% osmium tetroxide, stained with 0.8% potassium ferrocyanide, dehydrated, and embedded in EPON resin. Ultrathin sections collected on copper grids were stained with 2% uranyl acetate in water and lead citrate solution. Electron micrographs of skeletal muscle were taken using a Tecnai G2 F20 (FEI) 200 kV FEG with CCD Eagle 4kx4k transmission electron microscope. Thiery staining was performed with 1% periodic acid, 0.2% thiocarbohydrazyde (TCH) in 20% acetic acid and 1% silver proteinate (PATAg reaction). Electron microscopy images of the heart were taken using a Tecnai Spirit transmission electron microscope. TEM of glycogen purified particles was conducted on a 400-mesh grid, glow-discharged before use. Droplets of approx. 0.01% glycogen dispersed in distilled water were placed on the grid for ~1.5 min before staining with 2% aqueous uranyl acetate. The particles were imaged on a JEOL 1010 TEM (Tokyo, Japan) operating at 80 kV at the University of Barcelona, Spain. Particle size was measured by ImageJ software. All TEM analyses were successfully performed on samples from 3 animals per group, with a minimum of 15 pictures per sample analyzed by a blinded investigator.

Quantitative RT-PCR

Frozen tissues were homogenized by Polytron in TRIzol (Invitrogen), and mRNA was isolated using the RNeasy Mini kit (QIAGEN). Reverse transcription was performed using the Superscript one step TM RT-PCR System (Invitrogen). The following housekeeping genes were used: 18S and RPL13. Total DNA from tissues was extracted with the DNeasy Blood and Tissue Kit (QIAGEN). We quantified mitochondrial DNA by real-time PCR. Total DNA was used as a template and was amplified with specific oligodeoxynucleotides for mitochondrial DNA or Sdha (nuclear gene). We calculated the mitochondrial DNA copy number per cell by using Sdha amplification as a reference for nuclear DNA content. The primers used for qPCR are indicated in the supplemental information (Table S1).

Metabolite determination

Blood glucose levels were determined using a glucometer (Contour Next, Bayer Healthcare). Blood lactate was measured spectrophotometrically using a commercial kit (HORIBA ABX, Montpellier, France). The intracellular concentrations of ATP and other adenylates were measured from perchloric acid extracts of skeletal muscle tissue. They were quantified after HPLC in a Brisa column LC2 C18 (Teknokroma).

Respiration studies in permeabilized muscle

Soleus and EDL muscles were removed from the mice and placed in ice-cold isolation solution BIOPS (10 mM Ca-EGTA buffer [2.77 mM of CaK_2EGTA + 7.23 mM of K_2EGTA], 20 mM imidazole, 20 mM taurine, 50 mM K-Mes, 3 mM K_2HPO4, 6.5 mM $MgCl_2$, 5.7 mM ATP, 15 mM phosphocreatine, and 0.5 mM DTT [pH 7.1]). The addition of saponin (50 μg/mL) favored the permeabilization of single fibers that had previously been separated mechanically. After transferring the muscle bundles to a respiration medium (0.5 mM EGTA, 3 mM $MgCl_2 \cdot 6H_2O$, 20 mM taurine, 10 mM KH_2PO_4, 20 mM HEPES, 1 g/L BSA, 60 mM K-lactobionate, and 110 mM sucrose [pH 7.1]), high resolution respirometry was measured at 37°C by Oxygraph-2K (Oroboros instruments), as described (Sebastián et al., 2016). The following protocol was used: resting respiration (absence of adenylates, state 4), 10 mM glutamate and 2 mM malate (complex I), 2.5 mM ADP (state 3), 10 μM cytochrome *c* (integrity of the outer mitochondrial membrane), 10 mM succinate (state 3, complex I and II), and protonophore carbonylcyanide-4-(trifluoromethoxy)-phenylhydrazone (FCCP) (maximal O_2 flux).

Indirect calorimetry

An 8-chamber Oxymax system (Columbus Instruments) was used to measure O_2 consumption, CO_2 production, and other calorimetric parameters, as described in (López-Soldado et al., 2015). Briefly, measurements were taken after two days of acclimation for 2 cycles of 24 hr. Energy expenditure was calculated using the formula $(3.185 + 1.232 \times RER) \times V_{O2}$, where the respiratory exchange ratio (RER) = V_{CO2}/V_{O2}. Glucose oxidation in g/min/kg$^{0.75}$ was calculated using the formula $([4.545 \times V_{CO2}] - [3.205 \times V_{O2}])/1000$, and lipid oxidation in g/min/kg$^{0.75}$ was calculated using the formula $(1.672 \times [V_{O2} - V_{CO2}])/1000$. Locomotor activity was monitored by an infrared photocell beam interruption method.

Food intake, body temperature and weight

Food intake was monitored for five days in individually caged animals that were acclimatized for one week prior to the study. Total body fat and lean mass were monitored by EchoMRI-100 (EchoMRI, Houston, Texas).

Mass spectrometry

Frozen skeletal muscle was rapidly homogenized in 30% KOH at 4°C for 18 s at increasing polytron speed. Samples were boiled for 3 min at 100°C and quickly cooled in ice. These conditions were optimized to achieve an incomplete digestion of the glycogen bound proteins, so that the covalently bound peptides remain linked to glycogen.

Glycogen was precipitated with 66% EtOH (v/v) centrifuged, and re-suspended in water. This step was repeated five times. Samples were extracted using a 1:1 solution of acetonitrile and 1% formic acid, then sonicated for 5 min and centrifuged in order to extract the non-covalently bound peptides. The supernatant was then removed. These steps were repeated three times. Glycogen samples (which still contained the covalentlylinked peptides) were re-suspended in water for mass spectrometry applications and parallel glycogen measurement. Samples were added to a FASP filer unit (50-kDa cutoff) and glycogen was digested in the filter by amyloglucosidase for 96 hr at 37°C or by amylase for 72 hr at 37°C. Eluted peptides were analyzed by nanoLC-MS/MS. The sample volumes were reduced to approximately 15 μL in a vacuum centrifuge and were cleaned with PolyLC C18 pipette tips. The nanoLC-MS/MS was set up via the following steps. Digested peptides were first diluted in 1% FA. Samples were loaded onto a 180 μm × 2 cm C_{18} Symmetry trap column (Waters) at a flow rate of 15 μL/min using a nanoAcquity Ultra Performance LC chromatographic system (Waters, Milford, MA). Peptides were separated using a C_{18} analytical column (BEH130TM C_{18} 75 μm × 25 cm, 1.7 μm, Waters) with a 130 min run, comprising three consecutive steps with linear gradients from 1 to 35% B in 90 min, from 35 to 50% B in 15 min, and from 50 to 85% B in 2 min, followed by isocratic elution at 85% B in 10 min and stabilization to initial conditions (where A = 0.1% FA in water, B = 0.1% FA in CH3CN). The column outlet was directly connected to an Advion TriVersa NanoMate (Advion) fitted on an LTQ-FT Ultra mass spectrometer (Thermo). The spectrometer was working in positive polarity mode and in a data-dependent acquisition (DDA) mode. Singly charged precursors were rejected for fragmentation. Survey MS scans were acquired in the FT with the resolution (defined at 400 m/z) set to 100,000. Up to six of the most intense ions per scan were fragmented and detected in the linear ion trap. The ion count target value was 1,000,000 for the survey scan and 50,000 for the MS/MS scan. Target ions already selected for MS/MS were dynamically excluded for 30 s. Spray voltage in the NanoMate source was set to 1.70 kV. The capillary voltage and tube lens on the LTQ-FT were tuned to 40 V and 120 V, respectively. The minimal signal required to trigger MS to MS/MS switch was set to 1,000 and activation Q was 0.250. LC-MS/MS data analysis was performed with Proteome Discoverer software v1.4 (Thermo Scientific) using the Sequest HT search engine and SwissProt database (*Mus musculus*, amyloglucosidase from aspergillus niger and amylase [release 2014_07] and the common Repository of Adventitious Proteins [cRAP database]). Database searches were run against targeted and decoy databases. Search parameters included no-enzyme specificity, methionine oxidation, and 1 to 3 hexoses in serine, threonine, and tyrosine as dynamic modifications. Peptide mass tolerance was 10 ppm and the MS/MS tolerance was 0.6 Da. Peptides with a FDR < 1% were considered as positive identifications with a high confidence level. Detected peptides were validated manually.

Treadmill exercise

The animals were acclimatized to treadmill running (Columbus Instruments) for 5 min per day over 5 days at a speed between 10 and 14 cm/s and a slope of 0°. On the day of the experiment, animals ran on a treadmill with a 10° inclination, starting at a speed of 10 cm/s for 3 min. Every 2 min, the speed was increased by 2 cm/s until the mice were exhausted or a maximal speed of 46 cm/s was reached. A shock grid at the back of the treadmill was activated to prevent mice from stopping spontaneously. Exhaustion was defined as the inability of the animal to remain on the treadmill, and animals were removed from the treadmill after the following observations: 5 consecutive seconds on the shock grid without attempting to reengage the treadmill; spending more than 50% of the time on the shock grid; and willingness to sustain 2 s or more of shock rather than return to the treadmill on three occasions. Work was calculated as the product of body weight (kg), gravity (9.81 m/s^2), vertical speed (m/s; angle), and time (s). Power is the product of body weight (kg), gravity (9.81 m/s^2), and vertical speed (m/s; angle). On the day of the experiment, blood from the tail tip was taken for glucose and lactate measurements before and after exercise.

Myo-mechanical analysis of isolated muscles

Muscle mechanical properties were quantified *ex vivo,* as previously described (Pessina et al., 2014). Briefly, mice were sacrificed and muscles were rapidly excised into a dish containing oxygenated Krebs-Ringer solution. The commercially available 1200A isolated muscle test system (Aurora Scientific, ON, Canada) was used to assess muscle force. The optimum muscle length was determined by administering single electrical pulses while lengthening the muscle until the maximum isometric twitch force on single twitches was attained. Isometric-specific force was determined for each stimulation frequency (Hz) ranging from 1 to 200 Hz for 450 ms, with 1 min of rest between stimuli. Force was normalized to muscle weight and muscle fiber cross-sectional area *in vivo*, thereby calculating the specific net force (mN/mm^2).

QUANTIFICATION AND STATISTICAL ANALYSIS

Statistical Analysis

Results are presented as mean ± SEM of independent experiments. Unless otherwise indicated, significance between two variables was analyzed using a Student's t test, performed with the GraphPad Prism software (La Jolla, CA, USA). The following p values were considered to be statistically significant: p value $\leq$ 0.05 (*), p value $\leq$ 0.01 (**), and p value $\leq$ 0.001(***).

DATA AND SOFTWARE AVAILABILITY

The mass spectrometry proteomics data have been deposited in the ProteomeXchange Consortium via the PRIDE (Vizcaíno et al., 2016) partner repository, with the dataset identifier ProteomeXchange: PXD006377.